EARTH SCIENCES

Ocean heat drives rapid basal melt of the Totten Ice Shelf

Stephen Rich Rintoul,[1,2]* Alessandro Silvano,[2,3] Beatriz Pena-Molino,[1] Esmee van Wijk,[2] Mark Rosenberg,[1] Jamin Stevens Greenbaum,[4] Donald D. Blankenship[4]

Mass loss from the West Antarctic ice shelves and glaciers has been linked to basal melt by ocean heat flux. The Totten Ice Shelf in East Antarctica, which buttresses a marine-based ice sheet with a volume equivalent to at least 3.5 m of global sea-level rise, also experiences rapid basal melt, but the role of ocean forcing was not known because of a lack of observations near the ice shelf. Observations from the Totten calving front confirm that $(0.22 \pm 0.07) \times 10^6 \text{ m}^3 \text{ s}^{-1}$ of warm water enters the cavity through a newly discovered deep channel. The ocean heat transport into the cavity is sufficient to support the large basal melt rates inferred from glaciological observations. Change in ocean heat flux is a plausible physical mechanism to explain past and projected changes in this sector of the East Antarctic Ice Sheet and its contribution to sea level.

INTRODUCTION

Ice shelves form where the Antarctic Ice Sheet reaches the ocean and begins to float. Back stress produced by the interaction of the floating ice shelf with side walls and topographic rises buttresses the grounded ice sheet and inhibits the flow of ice into the ocean (1). The thinning or weakening of ice shelves reduces the back stress, increasing the discharge of grounded ice into the ocean and raising sea levels. The thinning of Antarctic ice shelves has been attributed to basal melt by ocean heat flux (2, 3), with the most rapid thinning, grounding line retreat, and acceleration of glacial flow observed in the Bellingshausen Sea and the Amundsen Sea (3, 4). Much of the ice sheet in that sector of Antarctica rests on bedrock below sea level that deepens upstream, a potentially unstable configuration that may result in rapid glacial retreat and mass loss to the ocean (5, 6). Models and observations suggest that increased ocean heat flux may have already initiated the unstable retreat of some West Antarctic glaciers (4, 7, 8). Therefore, the future evolution of the Antarctic Ice Sheet is tightly linked to change in the surrounding ocean.

Warm ocean waters make their closest approach to the Antarctic continent in the Bellingshausen Sea/Amundsen Sea sector (2, 9), and the most rapid warming of continental shelf bottom waters has occurred there (10), helping to explain the rapid mass loss from the West Antarctic Ice Sheet (WAIS). The WAIS has long been marine-based and susceptible to unstable retreat, whereas the East Antarctic Ice Sheet (EAIS) was assumed to be more stable as a result of its bedrock configuration and isolation from warm ocean waters. However, global sea-level rise in excess of 10 m during past warm climate epochs requires a substantial contribution from East Antarctica (11, 12). New observations have shown that large regions of the EAIS, including the Aurora Basin drained primarily by the Totten Glacier, are marine-based, with basal morphology (13) and sediment erosion records (14) that indicate repeated, large-scale advance and retreat of the ice sheet. The Totten Glacier drains more ice than any other glacier in the EAIS and contains a volume of marine-based ice above flotation equivalent to at least 3.5 m of global sea-level rise (15), comparable to that of the WAIS. The glacier occupies a deep fjord that connects to inland regions of retrograde

bed slope, conducive to rapid retreat, although the bed is flat or rises upstream immediately inland of the grounding line (16). Satellite altimetry and gravity measurements show that parts of the grounded portion of the EAIS have thinned in recent decades, with the most rapid changes observed at the Totten Glacier (17, 18). Evidence for recent change in the Totten Ice Shelf (TIS) is mixed: Laser altimetry indicated thinning from 2003 to 2008 (2), radar altimetry showed large temporal variability with no significant net volume loss between 1994 and 2012 (3), and a recent study found that the inferred mean basal melt rate for the period 2005–2011 was about one-third larger than the steady-state melt rate required to balance mass (19). Models suggest a substantial contribution to future sea-level rise from both the Wilkes Subglacial Basin and the Aurora Subglacial Basin in East Antarctica if greenhouse gas emissions remain high (20, 21). The modeled retreat of the Totten Glacier is initiated by simulated or assumed increases in ocean temperature, but the processes transporting ocean heat to ice shelf cavities are not well represented in coarse-resolution climate models. To date, no oceanographic measurements from the Totten ice front have been available to test the hypothesis that warm ocean waters can reach the ice shelf cavity and drive basal melt.

RESULTS

We collected oceanographic profiles and bathymetry data from the calving front of the TIS in January 2015 (Fig. 1; Materials and Methods). The heavy sea ice conditions that had prevented previous expeditions from reaching the ice front relaxed briefly during a period of southwest winds, allowing for access through a narrow and short-lived shore lead. Fast ice prevented access to the western 30 km of the ice front, where geophysical data (15) indicate shallower seafloor depths (Fig. 1A). Temperature, salinity, and oxygen were measured from the sea surface to within 8 m of the seafloor at 10 stations along the calving front and fast ice edge.

The shipboard bathymetry data reveal a deep trough in front of the western TIS cavity, with a maximum depth of 1097 m and a maximum width of 10 km at a depth of 600 m (Fig. 2A). Below 600 m, the trough narrows to form two deep channels with widths of 2 to 4 km. These narrow channels are much deeper than the BEDMAP2 estimate of bottom depth at the ice front [<350 m (22)]. Inversion of airborne geophysical data identified a trough in the same location as observed by the ship (Fig. 1A) but with a shallower maximum depth (<680 ± 190 m)

[1]Antarctic Climate and Ecosystems Cooperative Research Centre, University of Tasmania, Hobart, Tasmania, Australia. [2]Commonwealth Scientific and Industrial Research Organization Oceans and Atmosphere, Hobart, Tasmania, Australia. [3]Institute for Marine and Antarctic Studies, University of Tasmania, Hobart, Tasmania, Australia. [4]Institute for Geophysics, University of Texas at Austin, Austin, TX 78758, USA.
*Corresponding author. Email: steve.rintoul@csiro.au
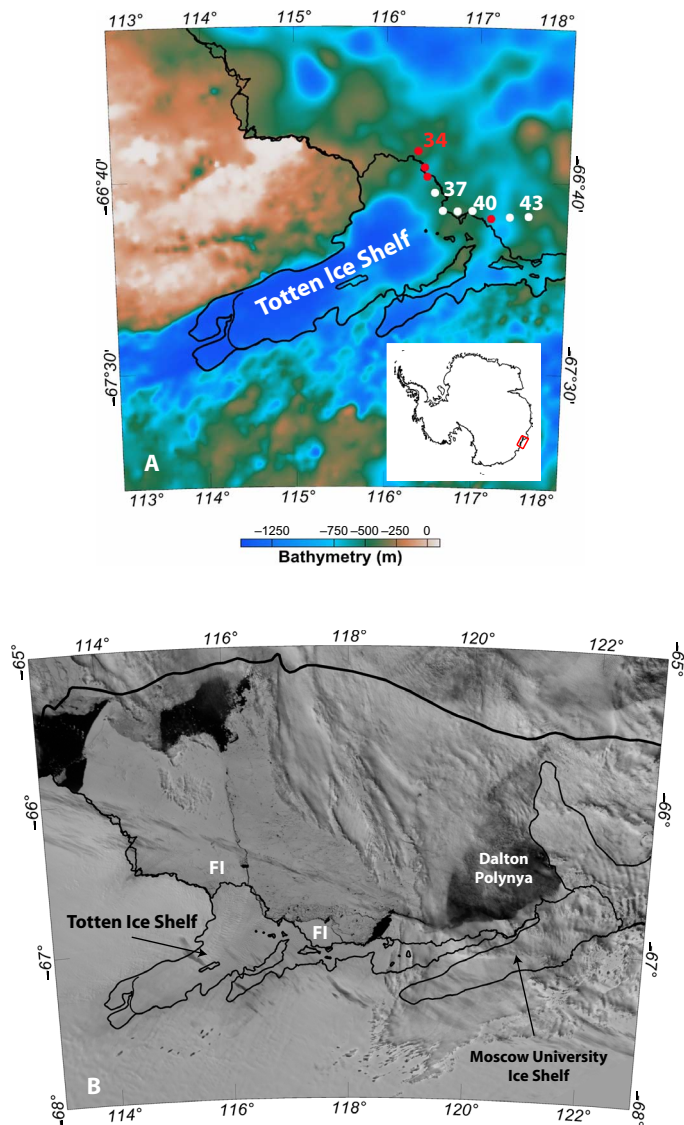
Fig. 1. Bathymetry, ice shelf draft, sea ice conditions, and ocean station locations near the Totten Glacier. (**A**) Seafloor bathymetry and elevation of the ice-rock interface, in meters above sea level, from airborne geophysical data (15). Dots indicate the locations of stations used in Fig. 2; red dots indicate stations where mCDW was detected; the grounding line shown in black was derived from interpretation of satellite data (34) updated with airborne radar data to indicate ocean access to the eastern part of the ice shelf (15). The coastline was derived from satellite radar imagery in 2004 (35). (**B**) Sea ice conditions on 7 January 2015 from Moderate Resolution Imaging Spectroradiometer (36). The outlines of the TIS, Moscow University Ice Shelf, and Antarctic continent are indicated by thin black lines. The continental shelf break is indicated by the heavy black line. Fast ice (FI) is present in front of the western and eastern limits of the TIS.

as a result of smoothing by the inversion procedure (15). The geophysical data indicate that the trough extends well south of the calving front and connects to the deep cavity beneath the TIS (Fig. 1A).

Warm modified Circumpolar Deep Water (mCDW) reaches the TIS cavity through these deep troughs (Fig. 2A). The warmest water is found at the seafloor at stations 34 and 35 [potential temperature (θ) = −0.405°C], with slightly cooler water (θ = −0.569°C) in the deepest

channel at station 36. A temperature maximum is also observed near the seafloor in a narrow channel further east (station 41), but the mCDW is much cooler there (maximum of −1.147°C) than that observed in the deep channel at stations 35 and 36. The channel at station 41 and that between stations 41 and 42 to the eastern trough identified by Greenbaum et al. (15) (Fig. 1A), representing the probable conduits for ocean heat to reach this eastward extension of the TIS.

The warm water in the deep trough is saline and low in oxygen, characteristic signatures of mCDW (Fig. 2, B and C). The Winter Water (WW) overlying the mCDW is cooler, fresher, and higher in oxygen. However, the salinity and oxygen of WW are lower (by >0.03 and >10 µM, respectively) in front of the western ice shelf than those observed further east, consistent with outflow from the ice shelf cavity of a mixture of low-oxygen mCDW and fresh glacial meltwater. Additional meltwater outflow may occur in the inaccessible area west of station 34.

The temperature of the mCDW near the seafloor in the deep trough exceeds the in situ freezing point by more than 2.2°C (the in situ freezing point decreases with increasing pressure) (Fig. 3A). If this warm water can access the grounding line at a depth of 2300 m (15), the temperature would exceed the local freezing point at the grounding line by 3.2°C. Velocity measurements collected by a lowered acoustic Doppler current profiler (LADCP) confirm that the warm water at the bottom of stations 35 and 36 flows strongly (>0.2 m s^{-1}) into the sub–ice shelf cavity (Fig. 3B). The velocity profile is highly sheared, with weak flow in the cold water above the thermocline near 600 m depth and maximum inflow near the seafloor, where the warmest water is found. The deep flow in the eastern trough (station 41) also flows into the cavity but is substantially weaker (Fig. 3B).

Integration of the along-trough velocity gives an inflow of 0.22 ± 0.07 Sv of warm (θ > −1.0°C) water at stations 34 to 36 (Materials and Methods). The LADCP provides a synoptic snapshot of the velocity field and may be aliased by tides or other motions; the error bar represents the uncertainty in the synoptic snapshot assuming a ±0.05 m s^{-1} barotropic tide (Materials and Methods). Although the representativeness of the LADCP-based transports cannot be assessed from direct observations, estimates of net basal melt inferred from glaciological measurements can be combined with temperature measured at the ice front to provide an independent estimate of the exchange rate [Materials and Methods (23)]. Glaciological estimates of basal melt at the Totten range from 63.2 ± 4 gigatons (Gt) year^{-1} (24) to 80 ± 5 Gt year^{-1} (19), the largest (24, 25) or the second largest [after the Amery (19)] basal melt rate for East Antarctic ice shelves with an area >1000 km^2. On an area-averaged basis, the Totten melt rate [10.5 ± 0.7 m year^{-1} in the study of Rignot et al. (24) and 9.89 ± 1.92 m year^{-1} in the work of Depoorter et al. (25)] is higher than that of any other East Antarctic ice shelf larger than 1000 km^2. Using the temperature of the inflow and outflow layers observed at the ice front, an overturning exchange flow of 0.16 ± 0.03 sverdrup is required to provide sufficient heat to support the inferred basal melt rate (Materials and Methods). The agreement within errors of the two independent transport estimates (0.22 ± 0.07 sverdrup from instantaneous velocity measurements and 0.16 ± 0.03 sverdrup from the multiyear mean basal melt rate), despite the different time periods and assumptions made, demonstrates that the observed water properties and circulation are consistent with high basal melt rates inferred from satellite data. Although ocean heat transport to the cavity likely varies in response to local and remote forcing (26, 27), the fact that the observed ocean heat flux is sufficient to support the multiyear mean basal melt rate derived from glaciological observations suggests that the conditions measured during the voyage were representative.
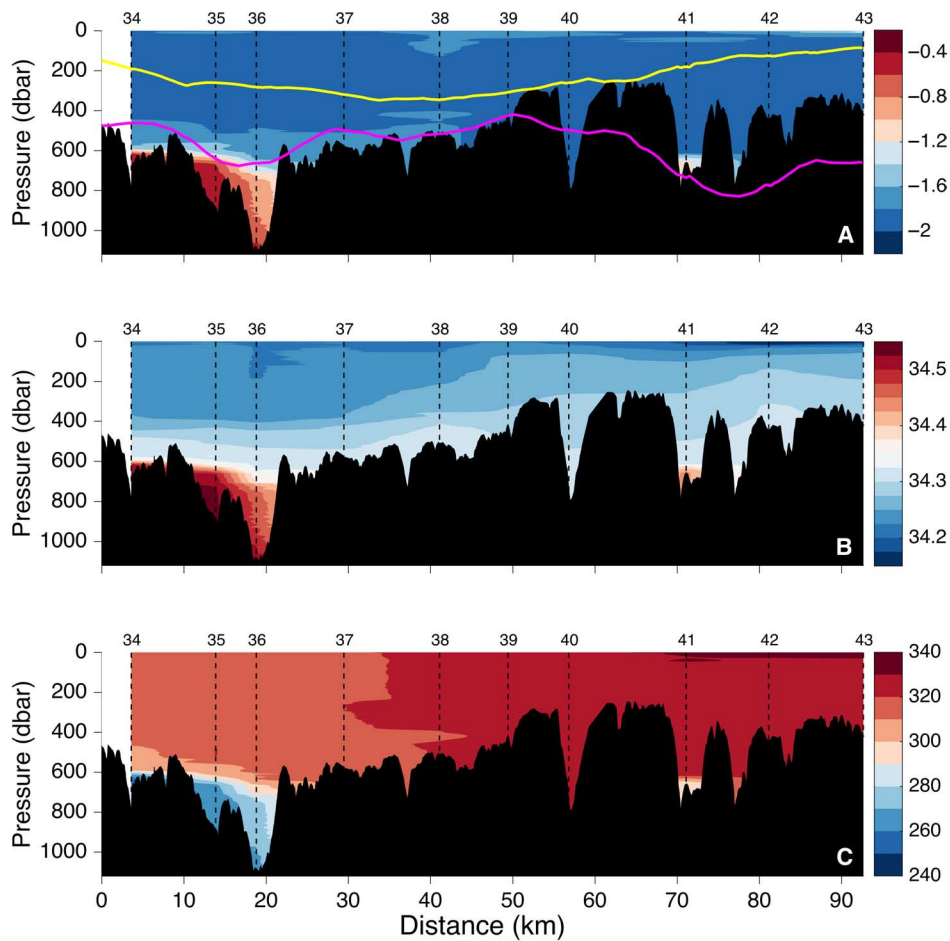
Fig. 2. Ocean properties along the TIS calving front. (**A**) Section of potential temperature (in degrees Celsius, color) and observed seafloor bathymetry (black) running from west (left) to east (right) along the calving front. The yellow line indicates the BEDMAP2 bathymetry (22); the magenta line shows the seafloor depth inferred from airborne geophysical measurements (15). (**B**) Salinity. (**C**) Oxygen (in micromolar).
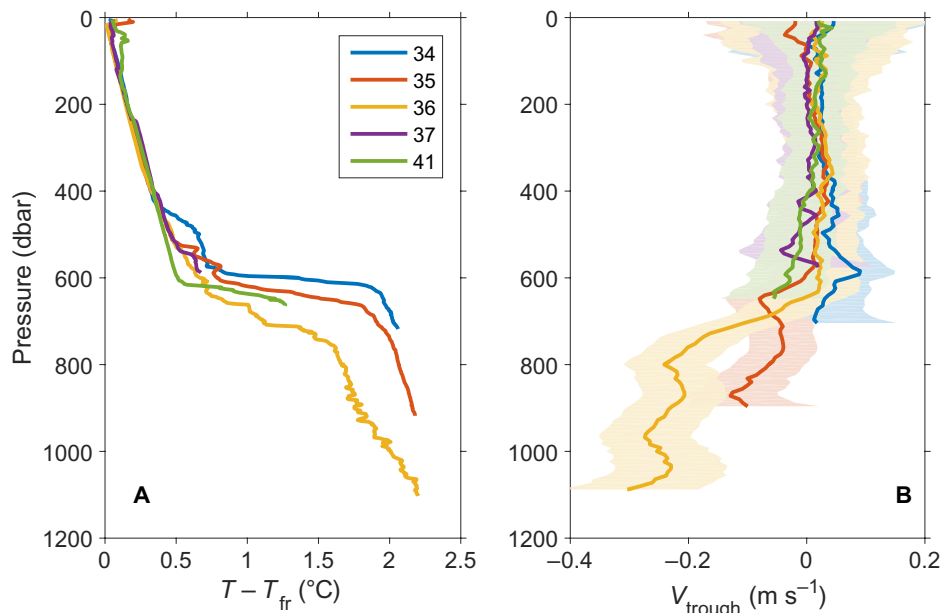
Fig. 3. Temperature above freezing and along-trough velocity. (**A**) Temperature elevation above the in situ freezing point at stations 34 to 37 (western trough) and 41 (eastern trough). (**B**) Velocity from the LADCP rotated in the along-trough direction [35° east of north for the western trough (stations 34 to 37) and 0° for the eastern trough (station 41) (15)].

CONCLUSION

Therefore, several lines of evidence support the conclusion that rapid basal melt of the TIS (19, 24, 25) is driven by the flux of warm mCDW into the cavity: the presence of warm water at the ice front, the existence of a deep trough providing access of this warm water to the cavity, direct measurements of mass and heat transport into the cavity, the signature of glacial meltwater in the outflow, and exchange rates inferred from the heat budget and satellite-derived basal melt rates. Observations of recent change in some East Antarctic glaciers and ice shelves (16–19) and studies of past (12–14, 28, 29) and future (20, 21) sea levels support the hypothesis of a dynamic EAIS. Our observations confirm the existence of a pathway allowing for communication of ocean anomalies to the TIS cavity, highlighting variation in ocean-driven basal melt as a plausible mechanism to explain past and projected changes in the TIS and the ice sheet it buttresses.

MATERIALS AND METHODS
Observations

Oceanographic profiles of temperature, salinity, and dissolved oxygen were collected using a Seabird 911 CTD with dual temperature and conductivity sensors and calibrated against bottle samples analyzed for salinity and oxygen. Velocity profiles were obtained with upward- and downward-looking LADCPs mounted on the CTD frame and an ADCP mounted in the hull of the ship. The LADCP data were processed using the inversion method of Visbeck (30) and Thurnherr (31). The LADCP velocity estimates were referenced using constraints from bottom-tracking, shipboard ADCP, and Global Positioning System position information. The inversion provided formal error bars (shown in Fig. 3); Thurnherr (32) argued that these formal error bars were often overly conservative. The shipboard ADCP was processed using the CODAS software package developed at the University of Hawaii (http://currents.soest.hawaii.edu/docs/adcp_doc/index.html).

Calculation of synoptic volume and heat transports

The transport of warm mCDW into the cavity was calculated by multiplying the LADCP velocity, rotated into the along-trough direction [35° east of north (15)], by the width of the channel in each 8-m-deep velocity bin and summing over the layer warmer than −1.0°C. [The −1.0°C isotherm lay roughly in the middle of the thermocline separating mCDW from WW; because the thermocline was sharp (~1.0°C/60 m), the transport integral was not sensitive to the temperature threshold chosen.] The LADCP measurements were potentially aliased by tides and other motions that were not resolved by the snapshot obtained by a single voyage. The tidal model of Padman et al. (33) suggested barotropic tidal velocities of less than ±0.015 m s^{-1} in this region, but tidal models are highly uncertain in this region of poorly known bathymetry. As a rough measure of uncertainty, we estimated the transport change resulting from a ±0.05 m s^{-1} barotropic tide and used this as an error bar on the volume transport. Heat transport into the cavity was estimated by multiplying the transport by the mean potential temperature in each 8-m-deep bin.

Multiyear fast ice prevented the ship from reaching the coast on the western end of the calving front. Airborne geophysical data indicated the seafloor shoals further west (15), suggesting that we have resolved the major inflows of warm mCDW. However, we likely missed some of the shallow outflow of glacial meltwater on the western end of the section. Hence, rather than directly integrating the LADCP velocity to calculate the outflow, we assumed that mass was conserved and that the total outflow must equal the total inflow plus meltwater input. (Note that we did not assume that the outflow and inflow were in the same vertical plane.)

We estimated the heat transport out of the cavity by multiplying the total outflow by the mean potential temperature in the layer with salinity less than 34.3 at stations 34 to 37. The difference between the ocean heat transport into and out of the cavity was the heat flux used to melt the base of the ice shelf. The heat flux estimated in this way was sufficient to produce 2.8 ± 0.9 mSv of meltwater.

Exchange estimated from satellite-derived basal melt

The transport calculation was based on a synoptic survey and may not represent the long-term mean exchange of volume and heat. The observed temperatures of the inflow and outflow layers could be used to provide an estimate of the volume exchange with the cavity that is independent of the velocity measurements. Following the study of Wilson and Straneo (23), we assumed a two-layer estuarine circulation in which warm water enters the cavity and drives basal melt, and a mixture of meltwater and mCDW leaves the cavity. Given a known basal melt rate and the temperature of the inflow and outflow, the heat budget can be used to estimate the exchange rate.

Several approaches have been used to estimate basal melt rates at the Totten Glacier. Flux gate calculations using satellite data indicated steady-state net basal melt rates of 63.2 ± 4 Gt year^{-1} (24) and 64 ± 12 Gt year^{-1} (25), equivalent to area-average melt rates of 10.5 ± 0.7 and 9.89 ± 1.92 m year^{-1}, respectively. The calculations were based on a number of data sets spanning different time periods and, thus, were best thought of as a multiyear average rather than an estimate for a particular time interval. Liu et al. (19) used a similar method, but did not assume a steady-state calving front as in the previous studies, and found a melt rate of 80 ± 5 Gt year^{-1} during the period 2005–2011. Numerical models gave net basal melt rates similar to these values [for example, 7 to 15 m year^{-1} (26) and 9.1 m year^{-1} with an interannual range of 5.7 m year^{-1} (27)]. We used the values from the study of Depoorter et al. (25) to estimate the exchange rate [Rignot (24) gave a similar value, with smaller error bars; using the melt rate of Liu et al. (19) would give a larger exchange rate, closer to our synoptic estimate].

The exchange rate is given by $M = L_f M_{melt}/c_w(T_{in} − T_{out})$, where M is the exchange rate, L_f is the latent heat of fusion (334 kJ kg^{-1}), c_w is the specific heat capacity of seawater (3.985 kJ kg^{-1} K^{-1}), M_{melt} is the flux of meltwater, and T_{in} and T_{out} are the potential temperatures of the inflow and outflow, respectively. A basal melt rate of 64 ± 12 Gt year^{-1} (25) corresponds to a meltwater flux M_{melt} of 2 ± 0.4 mSv. T_{in} is set to the transport-weighted temperature of the inflowing mCDW (−0.81°C). T_{out} is the mean temperature of the outflow layer at the calving front (−1.88°C). A meltwater flux of 2 ± 0.4 mSv requires an exchange rate M of 0.16 ± 0.03 Sv, assuming a two-layer flow with a temperature difference $T_{in} − T_{out} = 1.07$°C. A basal melt rate of 80 ± 5 Gt year^{-1} (19) equates to a meltwater flux of 2.5 ± 0.4 mSv, requiring an exchange rate M of 0.20 ± 0.03 Sv.

REFERENCES AND NOTES

1. T. K. Dupont, R. B. Alley, Assessment of the importance of ice-shelf buttressing to ice-sheet flow. *Geophys. Res. Lett.* **32**, L04503 (2005).
2. H. D. Pritchard, S. R. M. Ligtenberg, H. A. Fricker, D. G. Vaughan, M. R. van den Broeke, L. Padman, Antarctic ice-sheet loss driven by basal melting of ice shelves. *Nature* **484**, 502–505 (2012).
3. F. S. Paolo, H. A. Fricker, L. Padman, Volume loss from Antarctic ice shelves is accelerating. *Science* **348**, 327–331 (2015).

4. E. Rignot, J. Mouginot, M. Morlighem, H. Seroussi, B. Scheuchl, Widespread, rapid grounding line retreat of Pine Island, Thwaites, Smith, and Kohler glaciers, West Antarctica, from 1992 to 2011. *Geophys. Res. Lett.* **41**, 3502–3509 (2014).

5. J. Weertman, Stability of the junction of an ice sheet and ice shelf. *J. Glaciol.* **13**, 3–11 (1974).

6. C. Schoof, Ice sheet grounding line dynamics: Steady states, stability, and hysteresis. *J. Geophys. Res.* **112**, F03S28 (2007).

7. L. Favier, G. Durand, S. L. Cornford, G. H. Gudmundsson, O. Gagliardini, F. Gillet-Chaulet, T. Zwinger, A. J. Payne, A. M. Le BrocqFavier, Retreat of Pine Island Glacier controlled by marine ice-sheet instability. *Nat. Clim. Change* **4**, 117–121 (2014).

8. I. Joughin, B. E. Smith, B. Medley, Marine ice sheet collapse potentially under way for the Thwaites Glacier Basin, West Antarctica. *Science* **344**, 735–738 (2014).

9. A. H. Orsi, T. Whitworth III, W. D. Nowlin Jr., On the meridional extent and fronts of the Antarctic Circumpolar Current. *Deep Sea Res. Pt. I* **42**, 641–673 (1995).

10. S. Schmidtko, K. J. Heywood, A. F. Thompson, S. Aoki, Multidecadal warming of Antarctic waters. *Science* **346**, 1227–1231 (2014).

11. T. Naish, R. Powell, R. Levy, G. Wilson, R. Scherer, F. Talarico, L. Krissek, F. Niessen, M. Pompilio, T. Wilson, L. Carter, R. DeConto, P. Huybers, R. McKay, D. Pollard, J. Ross, D. Winter, P. Barrett, G. Browne, R. Cody, E. Cowan, J. Crampton, G. Dunbar, N. Dunbar, F. Florindo, C. Gebhardt, I. Graham, M. Hannah, D. Hansaraj, D. Harwood, D. Helling, S. Henrys, L. Hinnov, G. Kuhn, P. Kyle, A. Läufer, P. Maffioli, D. Magens, K. Mandernack, W. McIntosh, C. Millan, R. Morin, C. Ohneiser, T. Paulsen, D. Persico, I. Raine, J. Reed, C. Riesselman, L. Sagnotti, D. Schmitt, C. Sjunneskog, P. Strong, M. Taviani, S. Vogel, T. Wilch, T. Williams, Obliquity-paced Pliocene West Antarctic Ice Sheet oscillations. *Nature* **458**, 322–328 (2009).

12. K. G. Miller, J. D. Wright, J. V. Browning, A. Kulpecz, M. Kominz, T. R. Naish, B. S. Cramer, Y. Rosenthal, W. R. Peltier, S. Sosdian, High tide of the warm Pliocene: Implications of global sea level for Antarctic deglaciation. *Geology* **40**, 407–410 (2012).

13. D. A. Young, A. P. Wright, J. L. Roberts, R. C. Warner, N. W. Young, J. S. Greenbaum, D. M. Schroeder, J. W. Holt, D. E. Sugden, D. D. Blankenship, T. D. van Ommen, M. J. Siegert, A dynamic early East Antarctic Ice Sheet suggested by ice-covered fjord landscapes. *Nature* **474**, 72–75 (2011).

14. A. R. A. Aitken, J. L. Roberts, T. D. van Ommen, D. A. Young, N. R. Golledge, J. S. Greenbaum, D. D. Blankenship, M. J. Siegert, Repeated large-scale retreat and advance of Totten Glacier indicated by inland bed erosion. *Nature* **533**, 385–389 (2016).

15. J. S. Greenbaum, D. D. Blankenship, D. A. Young, T. G. Richter, J. L. Roberts, A. R. A. Aitken, B. Legresy, D. M. Schroeder, R. C. Warner, T. D. van Ommen, M. J. Siegert, Ocean access to a cavity beneath Totten Glacier in East Antarctica. *Nat. Geosci.* **8**, 294–298 (2015).

16. X. Li, E. Rignot, M. Morlighem, J. Mouginot, B. Scheuchl, Grounding line retreat of Totten Glacier, East Antarctica, 1996 to 2013. *Geophys. Res. Lett.* **42**, 8049–8056 (2015).

17. H. D. Pritchard, R. J. Arthern, D. G. Vaughan, L. A. Edwards, Extensive dynamic thinning on the margins of the Greenland and Antarctic Ice Sheets. *Nature* **461**, 971–975 (2009).

18. C. Harig, F. J. Simons, Accelerated West Antarctic ice mass loss continues to outpace East Antarctic gains. *Earth Planet. Sci. Lett.* **415**, 134–141 (2015).

19. Y. Liu, J. C. Moore, X. Cheng, R. M. Gladstone, J. N. Bassis, H. Liu, J. Wen, F. Hui, Ocean-driven thinning enhances iceberg calving and retreat of Antarctic ice shelves. *Proc. Natl. Acad. Sci. U.S.A.* **112**, 3263–3268 (2015).

20. N. R. Golledge, D. E. Kowalewski, T. R. Naish, R. H. Levy, C. J. Fogwill, E. G. W. Gasson, The multi-millennial Antarctic commitment to future sea-level rise. *Nature* **526**, 421–425 (2015).

21. R. M. DeConto, D. Pollard, Contribution of Antarctica to past and future sea-level rise. *Nature* **531**, 591–597 (2016).

22. P. Fretwell, H. D. Pritchard, D. G. Vaughan, J. L. Bamber, N. E. Barrand, R. Bell, C. Bianchi, R. G. Bingham, D. D. Blankenship, G. Casassa, G. Catania, D. Callens, H. Conway, A. J. Cook, H. F. J. Corr, D. Damaske, V. Damm, F. Ferraccioli, R. Forsberg, S. Fujita, Y. Gim, P. Gogineni, J. A. Griggs, R. C. A. Hindmarsh, P. Holmlund, J. W. Holt, R. W. Jacobel, A. Jenkins, W. Jokat, T. Jordan, E. C. King, J. Kohler, W. Krabill, M. Riger-Kusk, K. A. Langley, G. Leitchenkov, C. Leuschen, B. P. Luyendyk, K. Matsuoka, J. Mouginot, F. O. Nitsche, Y. Nogi, O. A. Nost, S. V. Popov, E. Rignot, D. M. Rippin, A. Rivera, J. Roberts, N. Ross, M. J. Siegert, A. M. Smith, D. Steinhage, M. Studinger, B. Sun, B. K. Tinto, B. C. Welch, D. Wilson, D. A. Young, C. Xiangbin, A. Zirizzotti, Bedmap2: Improved ice bed, surface and thickness datasets for Antarctica. *Cryosphere* **7**, 375–393 (2013).

23. N. J. Wilson, F. Straneo, Water exchange between the continental shelf and the cavity beneath Nioghalvfjerdsbræ (79 North Glacier). *Geophys. Res. Lett.* **42**, 7648–7654 (2015).

24. E. Rignot, S. Jacobs, J. Mouginot, B. Scheuchl, Ice shelf melting around Antarctica. *Science* **341**, 266–270 (2013).

25. M. A. Depoorter, J. L. Bamber, J. A. Griggs, J. T. M. Lenaerts, S. R. M. Ligtenberg, M. R. van den Broeke, G. Moholdt, Calving fluxes and basal melt rates of Antarctic ice shelves. *Nature* **502**, 89–92 (2013).

26. A. Khazendar, M. P. Schodlok, I. Fenty, S. R. M. Ligtenberg, E. Rignot, M. R. van den Broeke, Observed thinning of Totten Glacier is linked to coastal polynya variability. *Nat. Commun.* **4**, 2857 (2013).

27. D. E. Gwyther, B. K. Galton-Fenzi, J. R. Hunter, J. L. Roberts, Simulated melt rates for the Totten and Dalton ice shelves. *Ocean Sci.* **10**, 267–279 (2014).

28. C. P. Cook, T. van de Flierdt, T. Williams, S. R. Hemming, M. Iwai, M. Kobayashi, F. J. Jimenez-Espejo, C. Escutia, J. J. González, B.-K. Khim, R. M. McKay, S. Passchier, S. M. Bohaty, C. R. Riesselman, L. Tauxe, S. Sugisaki, A. Lopez Galindo, M. O. Patterson, F. Sangiorgi, E. L. Pierce, H. Brinkhuis, A. Klaus, A. Fehr, J. A. P. Bendle, P. K. Bijl, S. A. Carr, R. B. Dunbar, J. A. Flores, T. G. Hayden, K. Katsuki, G. S. Kong, M. Nakai, M. P. Olney, S. F. Pekar, J. Pross, U. Röhl, T. Sakai, P. K. Shrivastava, C. E. Stickley, S. Tuo, K. Welsh, M. Yamane, Dynamic behaviour of the East Antarctic Ice Sheet during Pliocene warmth. *Nat. Geosci.* **6**, 765–769 (2013).

29. A. Dutton, A. E. Carlson, A. J. Long, G. A. Milne, P. U. Clark, R. DeConto, B. P. Horton, S. Rahmstorf, M. E. Raymo, Sea-level rise due to polar ice-sheet mass loss during past warm periods. *Science* **349**, aaa4109 (2015).

30. M. Visbeck, Deep velocity profiling using lowered acoustic Doppler current profilers: Bottom track and inverse solutions. *J. Atmos. Oceanic Tech.* **19**, 794–807 (2002).

31. A. M. Thurnherr, A practical assessment of uncertainties in full-depth velocity profiles obtained with Teledyne/RDI Workhorse acoustic Doppler current profilers. *J. Atmos. Oceanic Tech.* **27**, 1215–1227 (2010).

32. A. M. Thurnherr, *How to Process LADCP Data with the LDEO Software, Versions IX.7–IX.10* (Lamont Doherty Earth Observatory, 2014).

33. L. Padman, H. A. Fricker, R. Coleman, S. Howard, L. Erofeeva, A new tide model for the Antarctic ice shelves and seas. *Ann. Glaciol.* **34**, 247–254 (2002).

34. E. Rignot, J. Mouginot, B. Scheuchl, Antarctic grounding line mapping from differential satellite radar interferometry. *Geophys. Res. Lett.* **38**, L10504 (2011).

35. J. Bohlander, T. Scambos, *Antarctic Coastlines and Grounding Line Derived from MODIS Mosaic of Antarctica (MOA)* (National Snow and Ice Data Center, 2007); http://nsidc.org/data/atlas/news/antarctic_coastlines.html.

36. T. Scambos, B. Raup, J. Bohlander, *Images of Antarctic Ice Shelves, Version 1* (National Snow and Ice Data Center, 2001); http://dx.doi.org/10.7265/N5NC5Z4N.